ISTFA™ 2022: Conference Proceedings from the 48th International Symposium for Testing and Failure Analysis
October 30–November 3, 2022
Pasadena Convention Center, Pasedena, California, USA
https://doi.org/10.31399/asm.cp.istfa2022p0181

Large Field of View and Artifact-free Plan View TEM Specimen Preparation by Post-FIB Ar Milling

C.S. Bonifacio, R. Li, P. Nowakowski, M.L. Ray, and P.E. Fischione
E.A. Fischione Instruments, Inc., Export, PA USA

Abstract

Semiconductor devices are decreasing in dimensions and currently comprise stacks of ultrathin layers as in a spin-transfer torque magnetoresistive random-access memory (STT-MRAM) device. For successful characterization by transmission electron microscopy (TEM) for failure analysis and device development, an accurate and controllable thinning of TEM specimens for is desirable. In this work, we combine plan view Ga focused ion beam (FIB) and post-FIB Ar milling preparation to prepare TEM specimens from a STT-MRAM device. Post-FIB Ar milling technique as a final polishing step of plan view TEM specimens was shown to prevent exposure of the tunnel barrier layer that can be damaged by the Ga FIB beam. We discuss the plan view FIB preparation, post-FIB Ar milling step and image analysis of the TEM images.

Introduction

The use of focused ion beam (FIB) systems for transmission electron microscopy (TEM) specimen preparation is prevalent due to the speed and locational accuracy of the tool during extraction and specimen thinning. Typical TEM specimens are cross-sectional specimens. Techniques for preparing a cross-section specimen in a FIB system are well known and straight forward. In contrast to cross-section specimen preparation techniques, a plan view specimen is prepared with the specimen parallel to the bulk sample surface. The choice of a plan view configuration, as opposed to a cross-section configuration, is relatively infrequent. Nonetheless, there are many advantages in using plan view specimens, especially for device failure analysis: the sample yields many repeating features on a single specimen [1] (unlike a small cross-section specimen) [2]; there is a higher probability of confining a defect due to the larger field of view [3]; and the feasibility of a direct correlation of microscale properties by scanning electron microscopy (SEM) techniques. An example pertinent to device failure analysis is the direct correlation of scanning electron microscopy (SEM) techniques, such as electron beam-induced current (EBIC), with TEM analyses.

Two approaches of plan view specimen preparation using the FIB include direct extraction of a large bulk of material from the sample's surface in the FIB [2][5] and mechanical treatment by initial bulk polishing before FIB slicing [6] [7]. The first method requires a protective layer on the region of interest (ROI) to protect the area from ion beam damage; this method can be time consuming due to the removal of a large amount of material during FIB preparation. However, the latter approach can hinder site-specificity because the specimen can only be prepared from the polished edge and is also time consuming due to the mechanical polishing step.

In this work, we present post-FIB polishing by concentrated ion beam (CIB) Ar milling of plan view TEM specimens. CIB Ar milling is used as a final thinning step for TEM specimens; it effectively removes amorphous and Ga implantation artifacts from FIB preparation [9]. By employing CIB Ar milling, mechanical treatment or adding a protective block prior to FIB preparation [5] are unnecessary. Furthermore, CIB Ar milling removes the initially deposited protective layer on the ROI and results in high quality specimens with pristine surfaces and large fields of view for TEM characterization. This work presents a novel plan view TEM preparation for atomic resolution imaging and analysis of grain boundary structure in semiconductor devices.

Discussion

The ROI in the STT-MRAM device is the tunnel barrier layer, specifically, the grain structure of polycrystalline MgO thin film. Characterization of the MgO grain boundaries on a plan view TEM specimen requires the removal of the free and reference multilayer stacks in the magnetic tunnel junction (MTJ) that surrounds the MgO film as in [12]. Because MgO film can be easily damaged by Ga or electron beam [13][14] and because of the MgO film thickness, controlled and artifact-free plan view specimens with thicknesses of less than 3 nm are required.

Cross-section and plan view TEM specimens from a STT-MRAM [28 nm eMRAM, Samsung] were prepared in a FIB system. Post-FIB CIB Ar milling was performed in the Model 1080 PicoMill® TEM specimen preparation system [Fischione Instruments] using the high-tilt method from our previous works [9][10], which resulted in controlled and reproducible sample preparation.

Cross-section specimen fabrication using the FIB

A cross-section specimen was prepared in a FIB system, which was followed by CIB milling to determine the thickness of the layers in the MTJ in which the MgO layer is found. Figures 1a-b show TEM images of the cross-section specimen before and after CIB milling. The resulting specimen was of high quality and suitable for high resolution TEM imaging of the MTJ (Figure 1c). After CIB milling, each layer of the MTJ (free layer, tunnel barrier with the MgO layer, and reference layer) and its interface were revealed. The MgO layer thickness was measured as 2 nm.

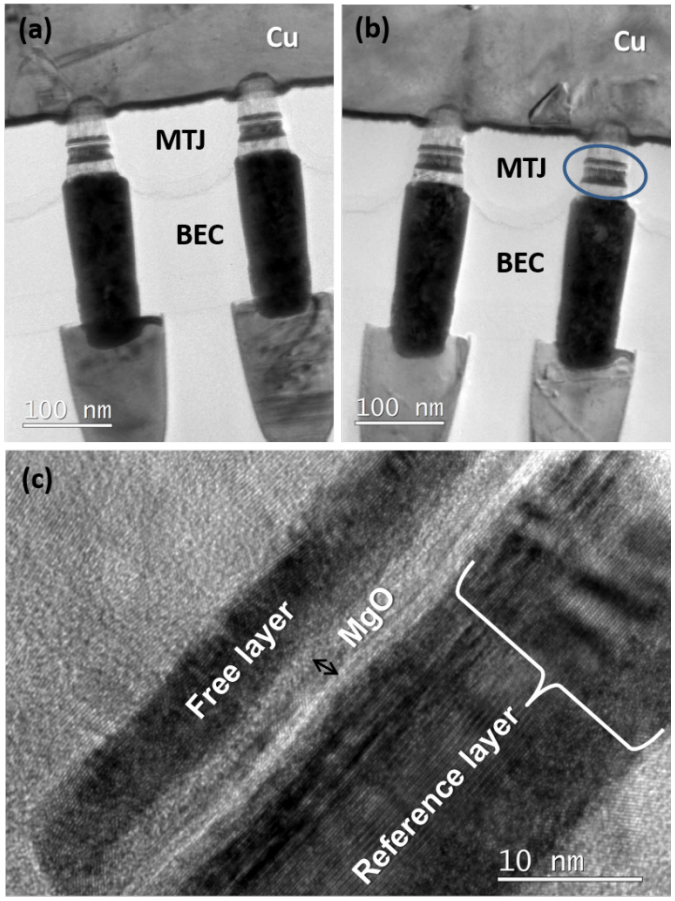

*Figure 1: TEM images of the STT-MRAM cross-section specimen (**a**) after FIB and (**b**) after concentrated Ar ion milling show the bottom electrode contact (BEC), magnetic tunnel junction (MTJ) and top Cu line of the STT-MRAM device. A high resolution TEM image (**c**) after Ar milling reveals the individual layers of the MTJ as free layer, tunnel barrier with MgO layer, and reference layer.*

The elemental composition of the MTJ layer was determined by energy dispersive X-ray spectroscopy (EDS). Figure 2 is a high angle annular dark field STEM image from which EDS was acquired. The free layer is a single layer composed of RuFeCo. The total tunnel barrier layer thickness is 3.5 nm and in the middle is the 2 nm thick MgO layer. Moreover, the reference layer is a multilayer stack composed of three layers: Co-rich FeCoRu, CoRu, and Ru-rich FeCoRu.

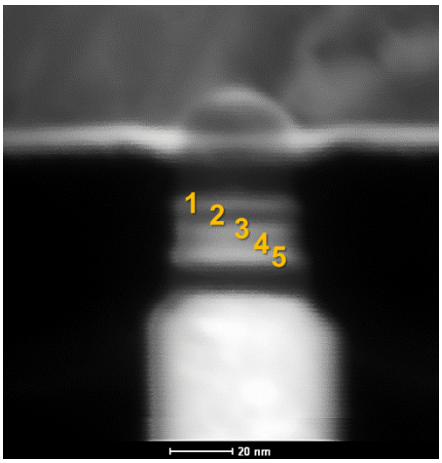

Layer	Material	Thickness [nm]
1	RuFeCo (Free layer)	5.0 nm
2	MgO (Tunnel barrier layer)	3.5 nm
3	CoRuFe (Reference layer)	6.0 nm
4	CoRu (Reference layer)	6.0 nm
5	RuCoFe (Reference layer)	6.0 nm

Figure 2. HAADF-STEM image of the STT-MRAM cross-section specimen with the layers of the MTJ identified from 1 to 5; the layer material type and thickness are summarized in the table.

Plan view specimen fabrication using the FIB

A Scios dual beam FIB [Thermo Fisher Scientific] was used where the electron source and Ga ion source traverse at 52°. A modified plan view FIB preparation from [2] was performed with the addition of Pt layer on the ROI without a flip stage. Figure 3a shows a SEM image of a pre-cut chunk of the STT-MRAM welded on a Cu grid with Pt deposited on top of the Cu metal line. It is imperative to deposit the Pt on the device to prevent Ga beam damage. Figures 3b-f are schematics of the plan view FIB preparation steps for the STT-MRAM device with the FIB parameters summarized in Table 1.

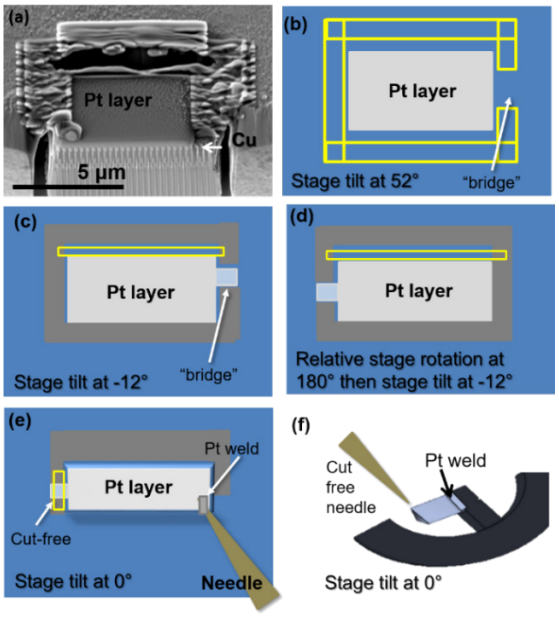

*Figure 3: Scanning electron microscopy top view image (**a**) of the STT-MRAM device with Pt deposited on top of the Cu metal layer. Plan view FIB specimen preparation steps are shown as illustrations (**b-f**) from the ion beam perspective with yellow boxes as milling patterns used during FIB milling.*

The bulk milling steps in Figure 3b require the depth of $z \geq 5$ µm to ensure that the ROI is within the chunk or specimen wedge to be prepared. Figures 3b-d result in a trapezoid-shaped specimen with a height equal to at least 5 µm. The trapezoid shape of the chunk is formed in Figures 3c-d while the stage is titled at -12°. Setting the depth to $z \geq 9$ µm ensures that chunk will be cut free in Figure 3d. In addition, the cleaning cross-section pattern was placed closer to the ROI side. The results shown in Figures 3c-d required a two-step process with the last step being the use of low current for cleanup. This ensures that the no part of the specimen chunk is touching the bulk specimen, which is necessary to successfully lift out the specimen chunk as shown in Figure 3e. As illustrated in Figure 3f, it is important that the grid is mounted with the flat side of the grid up and that the grid is flat (0°). Orienting the grid with the flat side up is important for ease in welding the specimen on the grid and for uniform milling of the specimen during the specimen polishing steps, respectively. When attaching the chunk to the grid, the grid and specimen chunk must both be in focus, which indicates that both are in the same plane. Aligning the specimen chunk to the grid required movement in the Z direction of the needle.

Table 1: Plan view specimen FIB preparation parameters for Figures b-f performed at 30 kV FIB voltage.

Figure 3	Purpose	Stage tilt	Stage rotation	Pattern type	Ion beam current
a	Pt deposition on the ROI with size dependent on the TEM specimen size	52°	0°	Rectangle	0.1 nA
b	"C shape" channel around the ROI to leave a small part of the sample or "bridge"	52°	0°	Regular cross-section with depth or $z \geq 5$ µm	15 nA, 7 nA
c	To make a wedge in long side of the specimen	-12°	0°	Cleaning cross-section with depth or $z \geq 9$ µm	5 nA, 3 nA
d	To make a wedge in long side of the specimen	-12°	180° from position in Figure 3c	Cleaning cross-section with depth or $z \geq 9$ µm	5 nA, 3 nA
e	Mount the specimen chunk to the needle with Pt and cut the specimen free from the bulk	0°	Same stage rotation as in Figure 3d	Rectangle	0.1 nA, 3 nA
f	Transfer, mount the specimen to the grid with Pt, and cut the needle free	0°	Same stage rotation as in Figure 3e	Rectangle	0.1 nA, 3 nA

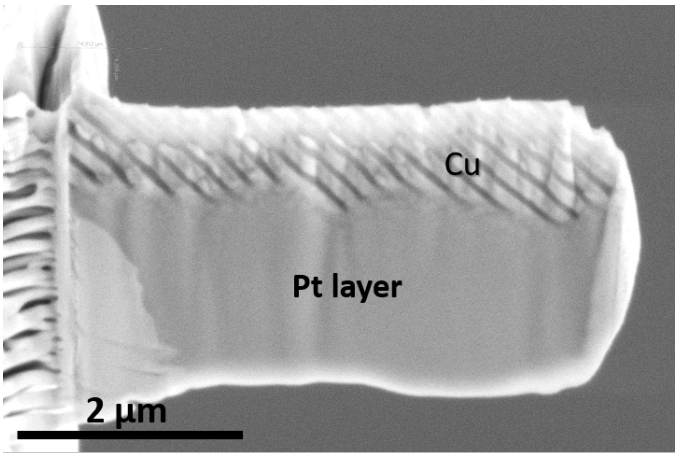

Figure 4: Scanning electron microscopy image of the SST-MRAM device plan view TEM specimen after thinning steps in the FIB. Part of the Pt layer was milled off, which exposed the Cu metal line.

Once the chunk was welded onto the grid, FIB polishing steps (summarized in Table 2) for thinning a TEM specimen were performed at 30 kV Ga with mostly at the back side of the specimen and significantly less at the front side with the Pt layer. Figure 3 shows the front side of the plan view TEM specimen after low kV thinning some of the Pt layer on the front side and mostly thinning of the specimen backside at 5 kV Ga (see Table 2).

Table 2: FIB specimen thinning parameters performed at 30 kV and 5 kV FIB voltages.

Orientation	Stage tilt	Pattern type	Energy and ion beam current
Back of specimen	51°	Cleaning cross-section with depth or Z = 2 µm	30 kV at: – 1 nA – 0.5 nA – 0.10 nA – 50 pA
Front of specimen with Pt layer	53°	Cleaning cross-section with depth or Z = 2 µm	30 kV at: – 0.5 nA – 0.10 nA – 50 pA
Front of specimen with Pt layer	55°	Rectangle	5 kV at 48 pA
Back of specimen	49°	Rectangle	5 kV and 48 pA

Post-FIB milling using a concentrated Ar ion beam

Final thinning of the specimen was performed using CIB Ar ion milling to remove the free and reference layers, which left only the MgO layer in the tunnel barrier layer. This step prevented the exposure of the MgO layer to the potentially damaging Ga ion beam during FIB preparation.

The CIB milling system, which has a 600 nm diameter Ar ion beam, was used to thin the FIB specimens to electron transparency. The system includes a LaB_6 electron source and electron detectors – a secondary electron detector (SED) and a scanning transmission electron microscope (STEM) – that provide in situ imaging during ion milling.

The grid with the FIB specimen was mounted on a specimen holder that is compatible with both the CIB milling system and the TEM. Following our previous work in [10], controlled and large area Ar ion milling specimens was achieved by high-tilt Ar milling. Figure 5 shows how the beam hits the specimen when it is tilted at 10°, as compared to a 15° tilt. By increasing the specimen tilt, the ROI is further exposed, which results in large electron transparent areas. The grid was mounted with the curved side of the grid on top. A user-defined milling box with size of 10 µm x 1 µm (width x height) was placed near the middle of the specimen; a small, concentrated beam of argon ions milled in a raster pattern within the box. The specimen was tilted 15° to mill the front side of the specimen. Decreasing energies were employed – 900 eV for the removal of the Pt layer to 700 eV for specimen thinning.

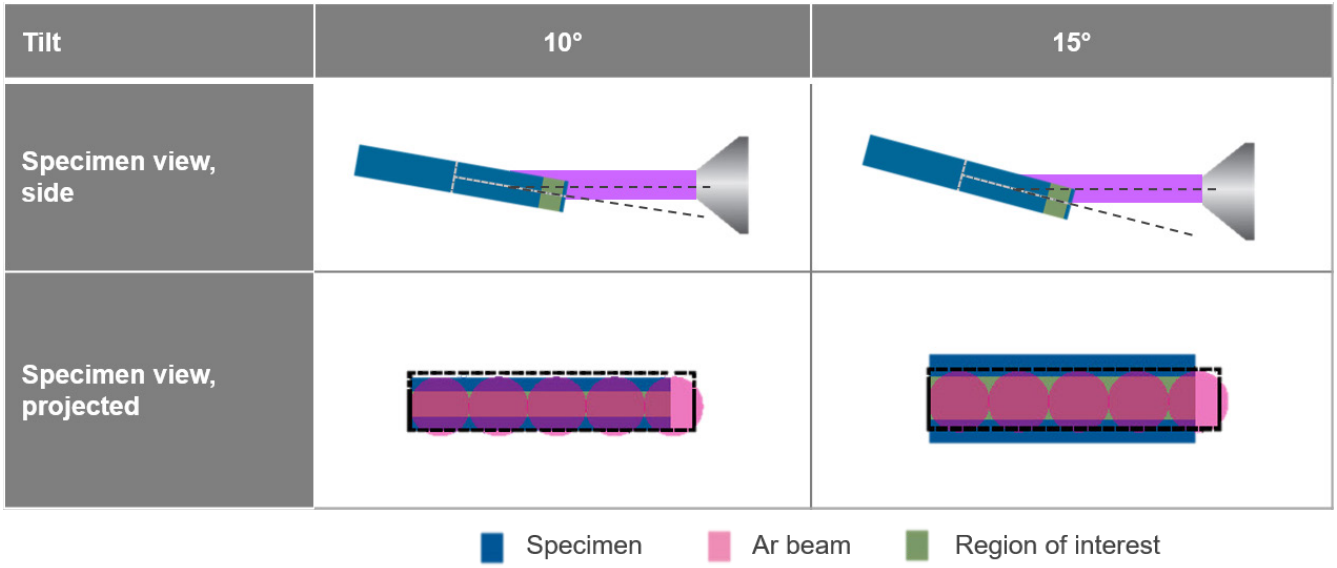

Figure 5: Relationship between Ar beam, specimen tilt (10 or 15°) and ROI on the specimen. Side view and projected view of the specimen with respect to the Ar beam show the increasing exposure of the ROI to the Ar beam as the specimen tilt increases.

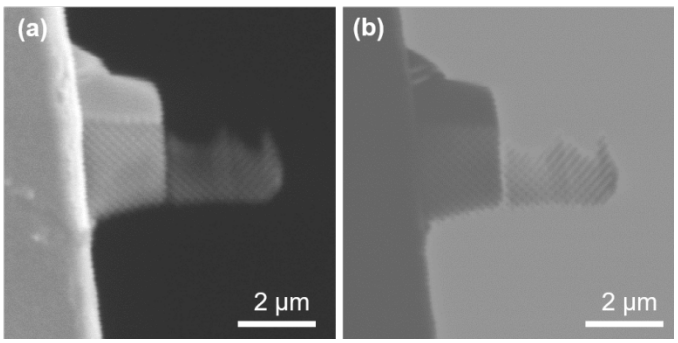

*Figure 6: Secondary electron detector (SED) image (**a**) and scanning transmission electron microscope (STEM) image (**b**) of the plan view TEM specimen acquired after post-FIB condensed ion beam Ar ion milling.*

Figure 6 shows electron transparency of the specimen after ion milling, which is especially visible in the STEM image (Figure 6b). The Pt protective layer is completely removed after Ar ion milling. Furthermore, the device structure is resolved (Figure 6), specifically the diagonal Cu metal lines across the specimen.

High-quality TEM specimens

The TEM images were acquired using a Tecnai F30 TEM [Thermo Fisher Scientific] equipped with an Orius charge-coupled device camera [Gatan] operated at 300 kV.

The initial plan view specimen after FIB preparation was more of a wedge; the bottom of the specimen was much thinner than the top. TEM imaging acquired after the removal of the Pt layer from the front side show the initial wedge specimen (Figure **7**a) with solid diagonal Cu lines and circular features from the MTJ layer distinguishable at the bottom left of the image. After 700 eV argon ion milling, the specimen was electron transparent (Figure **7**b).

Typically, light contrast in a bright field TEM image is attributed to areas enriched with low atomic number atoms, while the dark contrast is from high atomic number atoms. From this, the circular areas (marked with a blue box) are the tunnel barrier layer, which is comprised of a lighter element, MgO. The dark contrast in the TEM image, specifically the circular areas, correlated to the FeCoRu free and reference layers determined by EDS from the cross-section specimen (Figure 2). The layers of the MTJ structure were ascertained (Figure 7b): Cu metal line, light contrast circular areas with small grains inside, and dark contrast circular areas. Figure 7c shows four areas with the grains of MgO resolved and the SiO_2 layers in between the device structure free from redeposition.

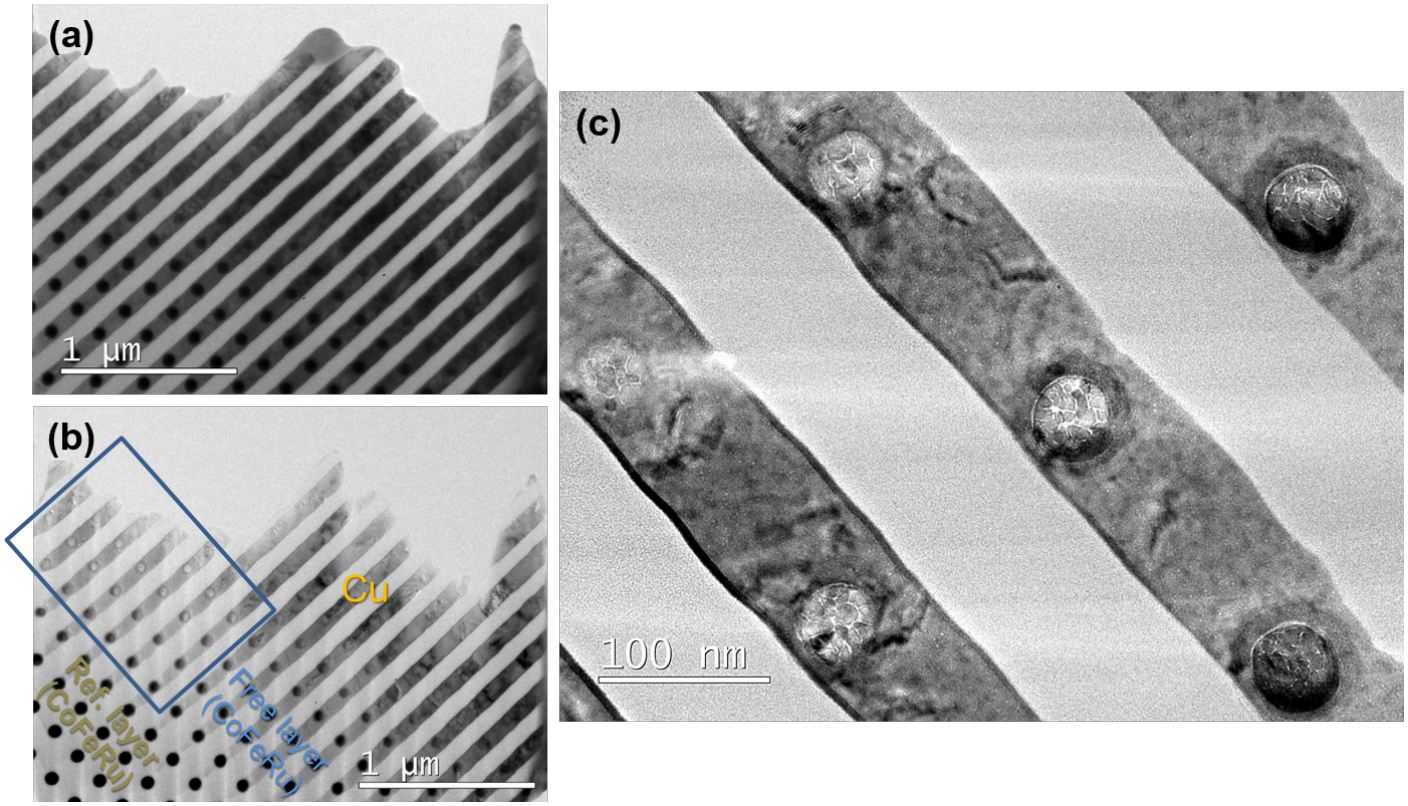

*Figure 7: Transmission electron microscope (TEM) images of the SST-MRAM plan view TEM specimen after 900 eV (**a**) and 700 eV (**b**) Ar ion milling show a slightly wedge-shaped specimen. The layers across the MTJ of the device (Cu, free layer, tunnel barrier layer, and reference layer) are identified (**b**). A high-magnification image (**c**) from the tunnel barrier layer (marked in **b**) displays multiple areas with resolved MgO grains.*

MgO verified by image analysis of HRTEM images

Further analysis of the HRTEM images was performed to confirm that Ar milling has removed the free layer on top and reference layer on the bottom of the MgO layer. Image analysis of HRTEM images used in previous studies [15, 16] was performed to determine the crystal phases and its location on a TEM image. Due to the large field of view of the specimen, multiple areas with possible MgO layer were imaged. The fast Fourier transform (FFT) from the HRTEM images reveals lattice spacings and directions that can be used to determine crystalline phase.

Figure 8a shows a HRTEM image from which an FFT was acquired (Figure 8b). By measuring the intensities on the FFT, lattice spacings and directions were compared for crystalline FeCo, FeCoB from the free and reference layers, and MgO from the tunnel barrier. The measured spacings were found to be equivalent to crystalline MgO (Figure 8b). An annular mask was superimposed on the intensities in the FFT equivalent to the measured radii of 1/2.46 $Å^{-1}$ and 1/1.51 $Å^{-1}$, corresponding to the (111) and (220) planes of MgO, respectively. To determine the spatial location of the corresponding crystal phase, the masked intensities in the FFT corresponding to (220) MgO planes (Figure 8c) were inverted with subsequent image threshold applied and selecting the lattice planes only. This process resulted to Figure 8d which revealed the position of individual MgO grains on the HRTEM image in Figure 8a. Figure 8e and f show the result of applying the mask on the (111) MgO planes and inverting the FFT followed by applying image threshold on the lattice planes.

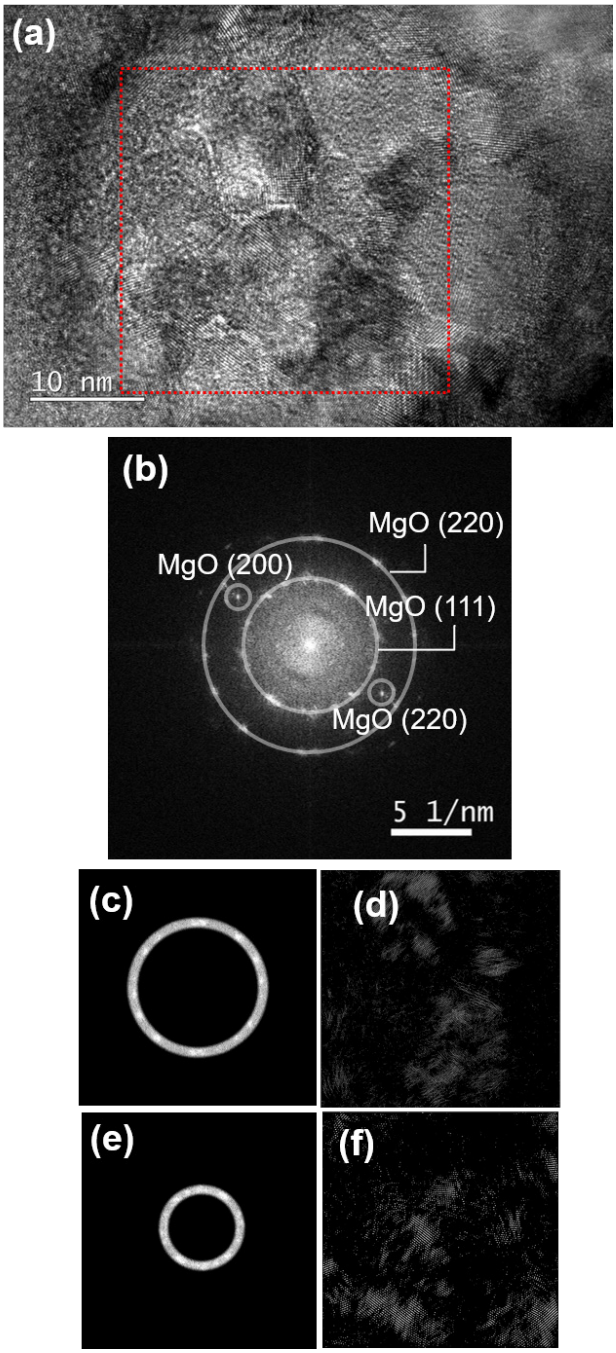

*Figure 8. High resolution transmission electron microscope (HRTEM) image of the SST-MRAM plan view TEM specimen after Ar milling (**a**) from which the fast Fourier transform (FFT) (**b**) was acquired. Intensities in the FFT (**b**) corresponded to MgO planes. Annular masks applied to the measured distance of 1/1.51 $Å^{-1}$ in (**c**) correspond to the (220) MgO plane with resulting inverse FFT (**d**), annular mask on the measured distance of 1/2.46 $Å^{-1}$ (**e**) correspond to the (111) MgO plane with resulting inverse FFT (**f**).*

The image analysis only focused on phases of MgO because there were no intensities matching the phases found in the free and reference layers. Consequently, the specific intensities from the MgO planes were highlighted with colored annular masks overlaid on the FFT shown in Figure 9a. These specific planes are then revealed by its spatial domain on the HRTEM image. The inverse FFTs from the MgO (111) and (220) planes were colorized accordingly (red and green) and superimposed on the HRTEM image. This provided the location of the thin MgO layer on the specimen as shown in Figure 9b and 9c. Based on the results, the tunnel free layer was covered with about 65% (Figure 9b) to 54% (Figure 9c) crystalline MgO across the circular area on the MTJ structure. Although the HRTEM images showed circular grain structures, part of these areas was found be amorphous based on the absence of lattice fringes and no intensities in the FFT detected. It can be inferred that the initially crystalline MgO grains became amorphous due to possible damage by the 300 kV beam during imaging in the TEM, as observed by previous work in [13].

Conclusions

Sample preparation of a STT-MRAM device using FIB to prepare a plan view specimen with post-FIB Ar ion milling was demonstrated. Successful preparation by CIB Ar ion milling of a plan view specimen without the need of mechanical polishing or a protective block prior to FIB preparation was established. Most importantly, novel sample preparation technique with post-FIB CIB Ar ion milling for final thinning step is presented without exposing the tunnel barrier layer with MgO to the damaging Ga beam. The result is high quality specimens with pristine surfaces and large fields of view for TEM characterization.

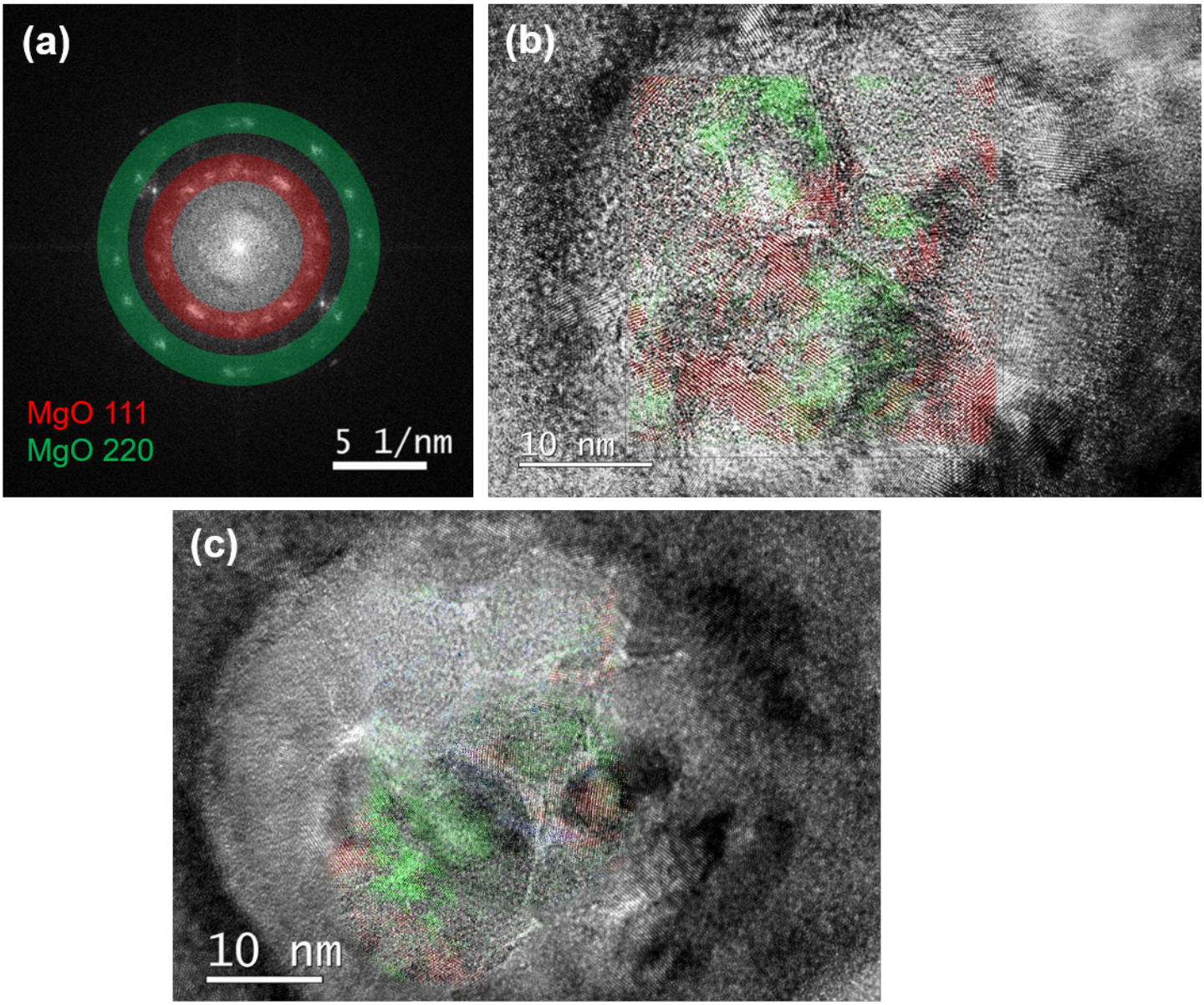

*Figure 9. Fast Fourier transform (FFT) superimposed with annular masks for the specific lattice MgO planes of (111) in red and (220) in green. The determined MgO lattice planes from the image analysis were superimposed on the corresponding high resolution transmission electron microscope (HRTEM) image (**b**) from which the FFT (**a**) was acquired. HRTEM image (**c**) is from another area analyzed showing location of the (111) and (220) MgO planes.*

References

[1] FA Stevie, RB Irwin, TL Shofner, SR Brown, JL Drown, and LA Giannuzzi (1998).”Plan view TEM sample preparation using the focused ion beam lift-out technique," AIP Conference Proceedings, 449, p. 868. https://doi.org/10.1063/1.56881.

[2] C Li, G Habler, LC Baldwin and R Abart (2018). “An improved FIB sample preparation technique for site-specific plan-view specimens: A new cutting geometry,” *Ultramicroscopy*, 184, p. 310.

[3] Zhu, J., Du, A. Y., Liu, B. H., Er, E., Zhao, S. P., & Lam, J. (2014). Tri-Directional TEM Failure Analysis on Sample Prepared by In-Situ Lift-Out FIB and Flipstage. *International Symposium for Testing and Failure Analysis*. https://doi.org/10.31399/asm.cp.istfa2014p0480

[4] Meyer, T., Westphal, T., Kressdorf, B., Ross, U., Jooss, C., & Seibt, M. (2021). Site-specific plan-view TEM lamella preparation of pristine surfaces with a large field of view. *Ultramicroscopy*, *228*, 113320. https://doi.org/10.1016/j.ultramic.2021.113320

[5] Jublot, M., & Texier, M. (2014). Sample preparation by focused ion beam micromachining for transmission

electron microscopy imaging in front-view. *Micron*, 56, 63–67. https://doi.org/10.1016/j.micron.2013.10.00

[6] O'Shea, K., McGrouther, D., Ferguson, C., Jungbauer, M., Hühn, S., Moshnyaga, V., & MacLaren, D. (2014). Fabrication of high quality plan-view TEM specimens using the focused ion beam. *Micron*, *66*, 9–15. https://doi.org/10.1016/j.micron.2014.04.011

[7] Anderson, R., & Klepeis, S. (1997). Combined Tripod Polishing and Fib Method for Preparing Semiconductor Plan View Specimens. *MRS Proceedings, 480*, 187. doi:10.1557/PROC-480-187

[8] Meyer, T., Westphal, T., Kressdorf, B., Ross, U., Jooss, C., & Seibt, M. (2021). Site-specific plan-view TEM lamella preparation of pristine surfaces with a large field of view. *Ultramicroscopy*, *228*, 113320. https://doi.org/10.1016/j.ultramic.2021.113320

[9] C. S. Bonifacio et al., "Cutting-edge sample preparation from FIB to Ar concentrated ion beam milling of advanced semiconductor devices," *Proc 46th Int'l Symp for Testing and Failure Analysis*, event cancelled, November 2020, p 133-140. doi:10.31399/asm.cp.istfa2020p0133

[10] C. Bonifacio et al., "High throughput and multiple length scale sample preparation for characterization and failure analysis of advanced semiconductor devices," *Proc 45th Int'l Symp for Testing and Failure Analysis*, Portland, OR, November 2019, p 295-301. doi:10.31399/asm.cp.istfa2019p0295

[11] C. Bonifacio et al., "Low energy Ar ion milling of FIB TEM specimens from 14 nm and future finFET technologies," *Proc 44th Int'l Symp for Testing and Failure Analysis*, Phoenix, AZ, October 2018, p 241-246. doi:10.31399/asm.cp.istfa2018p0241

[12] Bean, J. J., Saito, M., Fukami, S., Sato, H., Ikeda, S., Ohno, H., Ikuhara, Y., & McKenna, K. P. (2017). Atomic structure and electronic properties of MgO grain boundaries in tunnelling magnetoresistive devices. *Scientific Reports*, *7*(1). https://doi.org/10.1038/srep45594

[13] Harnchana, V., Brown, A. P., Brydson, R. M., Harrington, J. P., Hindmarch, A. T., Marrows, C. H., & Hickey, B. J. (2008, August). TEM characterization of a magnetic tunnel junction. *Journal of Physics: Conference Series*, 012058. https://doi.org/10.1088/1742-6596/126/1/012058

[14] Persson, A., Riddar, F., Nguyen, H., Ericson, F., & Thornell, G. (2011). *Ga Implantation in a MgO-based Magnetic Tunnel Junction With $Co_{60}Fe_{20}B_{20}$ Layers* (Vol. 47, Issue 1). Institute of Electrical and Electronics Engineers (IEEE). https://doi.org/10.1109/tmag.2010.2089634

[15] Holse, C., Elkjær, C. F., Nierhoff, A., Sehested, J., Chorkendorff, I., Helveg, S., & Nielsen, J. H. (2015). Dynamic Behavior of CuZn Nanoparticles under Oxidizing and Reducing Conditions. *The Journal of Physical Chemistry C*, *119*(5), 2804–2812. https://doi.org/10.1021/jp510015v

[16] Bonifacio, C. S., Liakakos, N., Salmeron, M., & Yang, J. C. (2016). Environmental TEM Studies of CoMn nanoalloys as Model Fischer-Tropsch Catalysts. *Microscopy and Microanalysis*, *22*(S3), 728-729.